ChemComm

Cite this: *Chem. Commun.*, 2011, **47**, 10945–10947

www.rsc.org/chemcomm

**COMMUNICATION**

# Characterization of a synthetic peroxodiiron(III) protein model complex by nuclear resonance vibrational spectroscopy†

**Loi H. Do,[a] Hongxin Wang,[bc] Christine E. Tinberg,[a] Eric Dowty,[d] Yoshitaka Yoda,[e] Stephen P. Cramer[bc] and Stephen J. Lippard*[a]**

*Received 27th June 2011, Accepted 28th July 2011*
**DOI: 10.1039/c1cc13836g**



**The vibrational spectrum of an $\eta^1,\eta^1$-1,2-peroxodiiron(III) complex was measured by nuclear resonance vibrational spectroscopy and fit using an empirical force field analysis. Isotopic $^{18}O_2$ labelling studies revealed a feature involving motion of the $\{Fe_2(O_2)\}^{4+}$ core that was not previously observed by resonance Raman spectroscopy.**

To understand better the molecular mechanisms of $O_2$ activation by carboxylate-bridged diiron enzymes,[1,2] it is desirable to determine the structures of intermediates that form in the process. Exposure of the $Fe^{II}_2$ cores of carboxylate-bridged diiron proteins to $O_2$ often generates transient peroxodiiron(III) intermediates.[3–9] Chart 1 depicts the possible coordination modes of a bridging $O_2^{2-}$ ligand at a dinuclear iron center.[1] Studies of such peroxo units in the R2 subunit of ribonucleotide reductase (RNR),[10,11] soluble methane monooxygenase hydroxylase (sMMOH),[12,13] toluene 4-monooxygenase hydroxylase (T4moH),[14] and $\Delta^9$ desaturase[15] have suggested that the reduced $O_2$ molecule is bound to the diiron core in an $\eta^1,\eta^1$-1,2 fashion. Recent quantum mechanical/molecular mechanics (QM/MM) investigations of the peroxo intermediates in the T201S mutant[16] of toluene/*o*-xylene monooxygenase hydroxylase (ToMOH)[17,18] favor formation of both $\eta^1,\eta^1$-1,2- and $\eta^1,\eta^1$-1,1-peroxodiiron(III) species upon reaction of the diiron(II) centre with $O_2$. The peroxo ligand in the latter structure is believed to be protonated and further stabilized by hydrogen bonding to the nearby hydroxyl residue, perhaps with an intervening water molecule. Attempts to characterize the ToMOH intermediates by resonance Raman (rR) spectroscopy or X-ray crystallography have not yet been successful, however. Although QM/MM theoretical studies have provided some insight into the nature of these $\{Fe_2(O_2)\}^{4+}$ units,[16,19–23] new methods are required to study the protein intermediates directly.

Nuclear resonance vibrational spectroscopy (NRVS)[24–27] is a valuable methodology recently applied in bioinorganic chemistry. For example, NRVS has been used to assign metal–ligand vibrational modes of diatomic molecules coordinated to porphyrins[26,28,29] and to detect nitrosylated iron-sulfur clusters in proteins.[30,31] NRVS and density functional theoretical (DFT) studies of mononuclear Fe(III)–OOH[32] and Fe(IV)=O[33,34] compounds have provided insight into their distintive chemical properties. In the present communication we describe the results of a study to evaluate NRVS as a means to interrogate the binding modes of peroxide ion at diiron centers in oxygenated protein intermediates by investigating a well-defined *cis*-$\eta^1,\eta^1$-1,2-peroxodiiron(III) protein model complex, $[Fe_2(\mu\text{-}O_2)(N\text{-EtHPTB})(PhCO_2)](BPh_4)_2$ (**1**·$O_2$, where *N*-EtHPTB = anion of *N*,*N*,*N*′,*N*′-tetrakis(2-benzimidazoyl-methyl)-2-hydroxy-1,3-diaminopropane) (Chart 2).[35–37]

To determine iron-ligand modes that arise from the *N*-EtHPTB and benzoate groups, the parent diiron(II) complex[36] $[^{57}Fe_2(N\text{-EtHPTB})(PhCO_2)](BPh_4)_2$ (**1**) was studied by NRVS. As shown in Fig. 1A (blue), polycrystalline **1** exhibits intense features in the 150 to 350 $cm^{-1}$ region of the spectrum. Because of the mixed ligand environment of **1**, this large envelope contains several overlapping Fe–N and Fe–O vibrations arising from benzimidazole, amine, alkoxide, and carboxylate units that are coordinated to the iron atoms. When a solution of **1** in tetrahydrofuran is exposed to dioxygen, a deep blue color rapidly develops, indicating generation of the peroxodiiron(III) complex **1**·$O_2$. The NRVS of **1**·$^{16}O_2$ and **1**·$^{18}O_2$ displayed intense bands between 150–300 $cm^{-1}$ (Fig. 1B and C, respectively, blue), assigned to iron-ligand (*N*-EtHPTB/$PhCO_2^-$) modes. In addition to these features, higher frequency bands at 338 and 467/480 $cm^{-1}$ were observed for **1**·$^{16}O_2$, where the latter two peaks are attributed

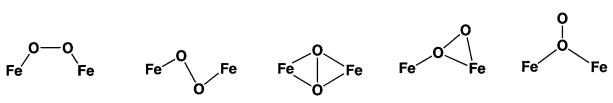


**Chart 1** Possible geometries of the ($\mu$-peroxo)diiron unit.

[a] *Department of Chemistry, Massachusetts Institute of Technology, 77 Massachusetts Avenue, Cambridge, MA 02139, USA. E-mail: lippard@mit.edu*
[b] *Department of Chemistry, University of California, Davis, CA 95616, USA. E-mail: spjcramer@ucdavis.edu*
[c] *Physical Biosciences Division, Lawrence Berkeley National Laboratory, Berkeley, CA 94720, USA*
[d] *Shape Software, 521 Hidden Valley Road, Kingsport, TN 37663, USA*
[e] *SPring-8/JASRI, 1-1-1 Kouto, Mikazuki-cho, Sayo-gun, Hyogo 679-5198, Japan*
† Electronic supplementary information (ESI) available. See DOI: 10.1039/c1cc13836g

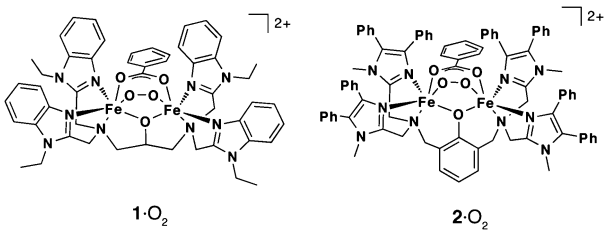


**Chart 2** A proposed structure of $[Fe_2(\mu\text{-}O_2)(N\text{-EtHPTB})(PhCO_2)]^{2+}$ (**1**·$O_2$, left). The benzoate ligand in **1**·$O_2$ may be coordinated in a terminal rather than bridging fashion.[37] The X-ray structure of $[Fe_2(\mu\text{-}O_2)(Ph\text{-bimp})(PhCO_2)]^{2+}$ (**2**·$O_2$, right) has been determined.[39]

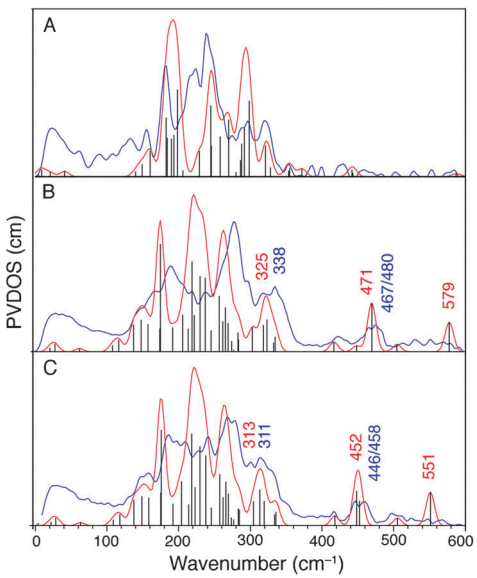


**Fig. 1** $^{57}$Fe partial vibrational density of states (PVDOS) for compounds **1**(A, 60 K, top), **1**·$^{16}O_2$ (B, 45 K, middle), and **1**·$^{18}O_2$ (C, 60 K, bottom) measured by NRVS. Color scheme: raw data in blue, empirical data fit in red, and individual eigenmode frequencies/intensities before broadening in black.

to Fermi splitting.[36] By comparison to the spectrum of **1** (Fig. 1A, blue), these higher energy modes of **1**·$O_2$ are probably due to motions involving the $\{Fe_2(O_2)\}^{4+}$ unit. Upon $^{18}O_2$-isotopic labelling, these features shifted to 311 and 446/458 $cm^{-1}$, respectively.

These results are consistent with previously reported resonance Raman spectra of **1**·$O_2$.[35,36] Most notably, the rR spectrum of **1**·$^{16}O_2$ exhibits bands at 466/474 $cm^{-1}$ that shift to a single peak at 452 $cm^{-1}$ upon substitution of $^{16}O_2$ with $^{18}O_2$ (Fig. S1A†). The 300–350 $cm^{-1}$ region of the rR spectrum does not show any resonance enhanced vibrations at the accessible excitation wavelengths (Fig. S1B†). The ability of NRVS to reveal a distinctive $\{Fe_2(O_2)\}^{4+}$ mode at 338 $cm^{-1}$, not previously observed for **1**·$^{16}O_2$ and shifting to 311 $cm^{-1}$ for **1**·$^{18}O_2$, illustrates the utility of this spectroscopic method.

To obtain a qualitative description of the modes that display significant $^{16}O_2/^{18}O_2$ isotopic shifts in the NRVS, normal coordinate analyses were performed for **1**·$^{16}O_2$ and **1**·$^{18}O_2$ using VIBRATZ.[38,39] To test the validity of the VIBRATZ simulations, the NRVS of **1** was calculated using the Cartesian coordinates of the diiron core from its X-ray crystal structure.[35] As shown by the red trace in Fig. 1A, the calculated spectrum reproduces the experimental one (blue) to a satisfactory first approximation. A complete assignment of this spectral region is beyond the scope of this study. Most importantly, the simulated NRVS of **1** does not show any peaks at energies greater than 350 $cm^{-1}$.

Because an X-ray structure of **1**·$O_2$ is not available, the geometry of its primary coordination sphere was modeled using the Cartesian coordinates from the X-ray structure of $[Fe_2(\mu\text{-}O_2)(Ph\text{-bimp})(PhCO_2)]^{2+}$ (**2**·$O_2$, Chart 2),[40] which has a ligand environment similar to that of **1**·$O_2$.[37] Although the structure of $[Fe_2(\mu\text{-}O_2)(N\text{-EtHPTB})(OPPh_3)_2]^{3+}$ (**3**·$O_2$) is known,[41] it has two triphenylphosphine oxide ligands rather than a benzoate group. The NRVS of **1**·$^{16}O_2$ and **1**·$^{18}O_2$ were simulated using the $\{Fe_2N_6O(\mu\text{-}O_2)(\mu\text{-}PhCO_2)\}^{2+}$ core of **2**·$O_2$ as a structural model (Fig. 1B and C, respectively, red traces). In agreement with experiment, the computed difference spectrum (**1**·$^{18}O_2$ minus **1**·$^{16}O_2$) showed that $^{18}O_2$ substitution should result in isotopically shifted peaks in the ~300–600 $cm^{-1}$ region (Fig. S2†). An additional isotope-sensitive mode was also calculated at 898 $cm^{-1}$ for **1**·$^{16}O_2$ and 847 $cm^{-1}$ for **1**·$^{18}O_2$, frequencies outside the window that was measured.

The highest energy calculated feature, at 898(817) $cm^{-1}$, is primarily a symmetric O–O stretching mode ($\nu_1$, Fig. 2). Because $\nu_1$ does not involve significant motion of the iron atoms, it is not likely to be very intense in the NRVS. The experimentally determined value for the symmetric $\nu$(O–O) mode of **1**·$O_2$ by rR spectroscopy, 897(847) $cm^{-1}$ (Fig. S1A†),[35,36] is in good agreement with the calculated one. The second highest energy mode falls at 579(551) $cm^{-1}$ and is essentially the asymmetric O–O stretching/rotation of the peroxo ligand against the iron atoms ($\nu_2$, Fig. 2). Although the net stretching of the Fe–O(peroxo) bonds is minimal, $\nu_2$ is expected to be observable by NRVS. The spectra of **1**·$O_2$, however, do not show any features in this region (Fig. 1B and C). It is possible that conformational heterogeneity or coupling with ligand vibrations, in a more complete model, may explain the absence of the feature at 579(551) $cm^{-1}$ in the NRVS. The weak bands at 513/532(500) $cm^{-1}$ in the rR spectrum[36] of **1**·$O_2$ (Fig. S2A†) might conceivably correspond to this $\nu_2$ mode.

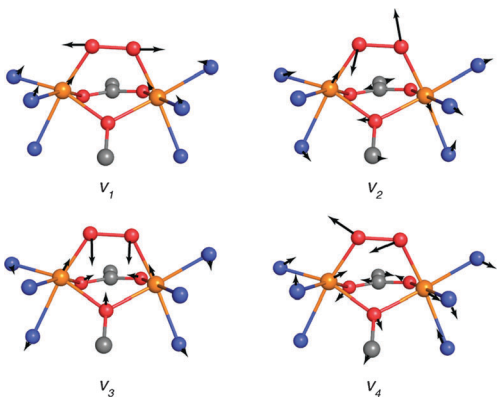


**Fig. 2** Normal mode calculations for **1**·$O_2$ using the X-ray coordinates of $[Fe_2(\mu\text{-}O_2)(Ph\text{-bimp})(PhCO_2)]^{2+}$ (**2**·$O_2$), showing the vibrations that involve the $\{Fe_2(O_2)\}^{4+}$ unit. The black arrows indicate the direction and relative degree of motion of the atoms to which they are attached. Color scheme: orange, iron; red, oxygen; blue, nitrogen; and gray, carbon.

The calculated peak at 471(452) $cm^{-1}$ ($\nu_3$) is attributed to the symmetric Fe–O–O–Fe stretching motion. The frequency of this mode depends almost entirely on the Fe–OO force constant (Fig. 2). The theoretical frequency of $\nu_3$ matches well those of **1**·$O_2$, observed at 467/480(446/458) $cm^{-1}$ in the NRVS (Fig. 1B and C) and at 466/474(452) $cm^{-1}$ in the rR spectra (Fig. S1A†).[36] Lastly, the isotopically shifted peak with lowest energy was calculated at 325(313) $cm^{-1}$ ($\nu_4$, Fig. 2). In this mode, the O–O group moves as a unit parallel to the Fe–Fe vector and perpendicular to the pseudo-mirror plane that bisects the $Fe_2(O_2)$ atoms. It is possible that the $\nu_4$ mode is absent in the rR spectrum because is it not strongly coupled to the electronic transition excited at 647 nm, the wavelength employed in the experiment.

In conclusion, the vibrational profile of a synthetic peroxodiiron(III) protein model complex has been revealed by nuclear resonance vibrational spectroscopy. Through $^{16}O_2/^{18}O_2$ isotopic labelling, the frequencies that correspond to motions of the $\{Fe_2(O_2)\}^{4+}$ unit in $[Fe_2(\mu\text{-}O_2)(N\text{-}EtHPTB)(PhCO_2)]^{2+}$ have been assigned. Most notably, a lower energy mode at ~338(311) $cm^{-1}$ involving parallel motion between the Fe–Fe and O–O groups has been detected by NRVS, a feature that was not previously observed by resonance Raman spectroscopy. Although a more comprehensive study is needed to correlate the vibrational characteristics of a peroxodiiron unit to its $O_2$ coordination geometry, these results demonstrate that synchrotron-based NRVS is a useful tool to interrogate the structure of oxygenated diiron protein intermediates. Such studies may help to clarify remaining questions regarding the mechanism of $O_2$ activation in carboxylated bridged diiron proteins.

The authors thank SPring-8 (JASRI, Proposal No. 2010A1600), the National Institute of General Medical Sciences (GM-65440 to SPC and GM-032134 to SJL), the NSF (CHE-0745353 to SPC), and the Department of Energy (DOE) Office of Biological and Environmental Sciences (to SPC) for supporting this work. Resonance Raman data were provided by Dr Takahiro Hayashi and Prof. Pierre Moënne-Loccoz.

## Notes and references

1 A. L. Feig and S. J. Lippard, *Chem. Rev.*, 1994, **94**, 759–805.
2 B. J. Wallar and J. D. Lipscomb, *Chem. Rev.*, 1996, **96**, 2625–2658.
3 D. E. Edmondson and B. H. Huynh, *Inorg. Chim. Acta*, 1996, **252**, 399–404.
4 K. E. Liu, D. Wang, B. H. Huynh, D. E. Edmondson, A. Salifoglou and S. J. Lippard, *J. Am. Chem. Soc.*, 1994, **116**, 7465–7466.
5 J. A. Broadwater, J. Ai, T. M. Loehr, J. Sanders-Loehr and B. G. Fox, *Biochemistry*, 1998, **37**, 14664–14671.
6 P. Moënne-Loccoz, C. Krebs, K. Herlihy, D. E. Edmondson, E. C. Theil, B. H. Huynh and T. M. Loehr, *Biochemistry*, 1999, **38**, 5290–5295.
7 L. J. Murray, S. G. Naik, D. O. Ortillo, R. García-Serres, J. K. Lee, B. H. Huynh and S. J. Lippard, *J. Am. Chem. Soc.*, 2007, **129**, 14500–14510.
8 V. V. Vu, J. P. Emerson, M. Martinho, Y. S. Kim, E. Münck, M. H. Park and L. Que, Jr., *Proc. Natl. Acad. Sci. U. S. A.*, 2009, **106**, 14814–14819.
9 V. K. Korboukh, N. Li, E. W. Barr, J. M. Bollinger, Jr. and C. Krebs, *J. Am. Chem. Soc.*, 2009, **131**, 13608–13609.
10 P. Moënne-Loccoz, J. Baldwin, B. A. Ley, T. M. Loehr and J. M. Bollinger, Jr., *Biochemistry*, 1998, **37**, 14659–14663.
11 A. J. Skulan, T. C. Brunold, J. Baldwin, L. Saleh, J. M. Bollinger, Jr. and E. I. Solomon, *J. Am. Chem. Soc.*, 2004, **126**, 8842–8855.
12 M. Merkx, D. A. Kopp, M. H. Sazinsky, J. L. Blazyk, J. Müller and S. J. Lippard, *Angew. Chem., Int. Ed.*, 2001, **40**, 2782–2807.
13 C. E. Tinberg and S. J. Lippard, *Acc. Chem. Res.*, 2011, **44**, 280–288.
14 L. J. Bailey and B. G. Fox, *Biochemistry*, 2009, **48**, 8932–8939.
15 J. A. Broadwater, C. Achim, E. Münck and B. G. Fox, *Biochemistry*, 1999, **38**, 12197–12204.
16 A. D. Bochevarov, J. Li, W. J. Song, R. A. Friesner and S. J. Lippard, *J. Am. Chem. Soc.*, 2011, **133**, 7384–7397.
17 F. L. G. Arenghi, D. Berlanda, E. Galli, G. Sello and P. Barbieri, *Appl. Environ. Microbiol.*, 2001, **67**, 3304–3308.
18 V. Cafaro, R. Scognamiglio, A. Viggiani, V. Izzo, I. Passaro, E. Notomista, F. Dal Piaz, A. Amoresano, A. Casbarra, P. Pucci and A. Di Dinato, *Eur. J. Biochem.*, 2002, **269**, 5689–5699.
19 E. A. Ambundo, R. A. Friesner and S. J. Lippard, *J. Am. Chem. Soc.*, 2002, **124**, 8770–8771.
20 M.-H. Baik, B. F. Gherman, R. A. Friesner and S. J. Lippard, *J. Am. Chem. Soc.*, 2002, **124**, 14608–14615.
21 B. D. Dunietz, M. D. Beachy, Y. Cao, D. A. Whittington, S. J. Lippard and R. A. Friesner, *J. Am. Chem. Soc.*, 2000, **122**, 2828–2839.
22 R. A. Friesner, M.-H. Baik, B. F. Gherman, V. Guallar, M. Wirstam, R. B. Murphy and S. J. Lippard, *Coord. Chem. Rev.*, 2003, **238-239**, 267–290.
23 D. Rinaldo, D. M. Philipp, S. J. Lippard and R. A. Friesner, *J. Am. Chem. Soc.*, 2007, **129**, 3135–3147.
24 W. Sturhahn, T. S. Toellner, E. E. Alp, X. Zhang, M. Ando, Y. Yoda, S. Kikuta, M. Seto, C. W. Kimball and B. Dabrowski, *Phys. Rev. Lett.*, 1995, **74**, 3832–3835.
25 W. R. Scheidt, S. M. Durbin and J. T. Sage, *J. Inorg. Biochem.*, 2005, **99**, 60–71.
26 W. Zeng, N. J. Silvernail, W. R. Scheidt and J. T. Sage, in *Nuclear Resonance Vibrational Spectroscopy, Application of Physical Methods to Inorganic and Bioinorganic Chemistry*, ed. R. A. Scott, C. M. Lukehart, Wiley, England, 2007, pp. 401–422.
27 W. Sturhahn, *J. Phys.: Condens. Matter*, 2004, **16**, S497–S530.
28 F. Paulat, T. C. Berto, S. DeBeer George, L. Goodrich, V. K. K. Praneeth, C. D. Sulok and N. Lehnert, *Inorg. Chem.*, 2008, **47**, 11449–11451.
29 N. Lehnert, M. G. I. Galinato, F. Paulat, G. B. Richter-Addo, W. Sturhahn, N. Xu and J. Zhao, *Inorg. Chem.*, 2010, **49**, 4133–4148.
30 Z. J. Tonzetich, H. Wang, D. Mitra, C. E. Tinberg, L. H. Do, F. E. Jenney, Jr., M. W. W. Adams, S. P. Cramer and S. J. Lippard, *J. Am. Chem. Soc.*, 2010, **132**, 6914–6916.
31 C. E. Tinberg, Z. J. Tonzetich, H. Wang, L. H. Do, Y. Yoda, S. P. Cramer and S. J. Lippard, *J. Am. Chem. Soc.*, 2010, **132**, 18168–18176.
32 L. V. Liu, C. B. Bell, III, S. D. Wong, S. A. Wilson, Y. Kwak, M. S. Chow, J. Zhao, K. O. Hodgson, B. Hedman and E. I. Solomon, *Proc. Natl. Acad. Sci. U. S. A.*, 2010, **107**, 22419–22424.
33 C. B. Bell, III, S. D. Wong, Y. Xiao, E. J. Klinker, A. L. Tenderholt, M. C. Smith, J.-U. Rohde, L. Que, Jr., S. P. Cramer and E. I. Solomon, *Angew. Chem., Int. Ed.*, 2008, **47**, 9071–9074.
34 S. D. Wong, C. B. Bell, III, L. V. Liu, Y. Kwak, J. England, E. E. Alp, J. Zhao, L. Que, Jr. and E. I. Solomon, *Angew. Chem., Int. Ed.*, 2011, **50**, 3215–3218.
35 Y. Dong, S. Ménage, B. A. Brennan, T. E. Elgren, H. G. Jang, L. L. Pearce and L. Que, Jr., *J. Am. Chem. Soc.*, 1993, **115**, 1851–1859.
36 L. H. Do, T. Hayashi, P. Moënne-Loccoz and S. J. Lippard, *J. Am. Chem. Soc.*, 2010, **132**, 1273–1275.
37 It has been proposed that the benzoate ligand in **1**·$O_2$ is bound in a terminal fashion rather than a bridging one. See: J. R. Frisch, V. V. Vu, M. Martinho, E. Münck and L. Que Jr, *Inorg. Chem.*, 2009, **48**, 8325–8336.
38 E. Dowty, *Phys. Chem. Miner.*, 1987, **14**, 67–79.
39 *Shape Software*, www.shapesoftware.com.
40 T. Ookubo, H. Sugimoto, T. Nagayama, H. Masuda, T. Sato, K. Tanaka, Y. Maeda, H. Ōkawa, Y. Hayashi, A. Uehara and M. Suzuki, *J. Am. Chem. Soc.*, 1996, **118**, 701–702.
41 Y. Dong, S. Yan, V. G. Young, Jr. and L. Que, Jr., *Angew. Chem., Int. Ed. Engl.*, 1996, **35**, 618–620.